

# Physics-Based Simulation of Vascular Trees for Surgery Simulations

Simon Adler

Fraunhofer IFF  
Magdeburg

adler@iff.fraunhofer.de

Tobias Moench

Dept. of Simulation and Graphics  
University of Magdeburg

tobias.moench@ovgu.de

Rüdiger Mecke

Fraunhofer IFF  
Magdeburg

mecke@iff.fraunhofer.de

## ABSTRACT

In minimal-invasive surgery there is a trend to interventions with even smaller instruments. These procedures are gentle for patients, but in many cases more complex for the surgeon. The new Single-Port Technique (SPT) enables the surgeon to perform an intervention through one incision point with several instruments. Nowadays, the SPT is applied only in selected surgeries. The application depends on the movement the surgeon can perform with the instrument in the region of interest. This depends on the patients specific anatomy and also on the design of the instruments. Virtual environments can support not only the training, but also the development of instruments adapted to new interventions. To estimate the possible movements and the residual degrees of freedom for the instruments, thus are inserted through one incision point, not only the organs are relevant, but also the vessels connecting them.

We present a method for the interactive physic based deformation of vascular systems during interaction. Therefore, the centerline of the vascular system is utilized for the physic based simulation and a surface representation is synchronized. Because the performance is a major issue and depends substantial on the surface resolution, so we also present a approach for the generation of a low resolution surface mesh for vascular systems whose resolution is adaptive to the vessels diameter.

## Keywords

Deformation, Surface Generation, Physics-based Simulation, Angular Spring, Surgery Simulation, Medical Simulation

## 1. INTRODUCTION

In minimal-invasive surgery interventions are performed with incisions of a few centimeters. In endoscopic surgery, three incision points are commonly used. Two for instruments and an additional one for the endoscopic camera. The Single-Port-Technique (SPT) aggregates these points into a single incision point, that is commonly located at the patients navel and called *the portal*. The pivots of the instruments are closely located, so the moving space for each individual instrument is restricted. This method, however, has advantages for the patient, but is quite new and nowadays applied in selected interventions. For a broader application of the SPT, new instruments optimized for more complex interventions are required. Therefore, it has to be verified if the degrees of freedom of an instrument are sufficient to accomplish the surgery. Virtual simulation environments can

support surgeons during training of new methods, but they can also support the development of instruments and the related examination of the achievable moving space and degree of freedom.

The scenario, targeted in our development, is the removal of the spleen (splenectomy) with the SPT. The spleen is difficult to reach via a single port. The location of the port and the operation strategy depend on the patients specific anatomy. Thus, such interventions may be very complex. The spleen is supplied with two main vessels buried within the patients fat. They pass other organs such as the stomach or the pancreas [6] closely and may be difficult to detect. Thus, important tasks during a splenectomy are the extraction and cutting of vessels, while an injury of surrounding anatomical structures should be avoided.

Virtual environments are used for the planning of difficult interventions. There are surgical simulation systems available, that a surgeon can use to train surgical procedures. The main challenge is the simulation of complex tissue deformations in real-time. For the liver, different simulation models are achieved to simulate its complex tissue behavior, but vessels are only considered if they have high relevance during the performed surgery.

However, vessels are important to verify the degrees of freedom and the movement space of instruments at a port, since surgeons need to reach the vessels for coagulation. Furthermore, vessels may interactively be moved by means of deformation if regions located behind have to be reached.

In medical visualization, the location of vascular structures can be identified from tomographic image data acquired via, computed tomography angiography (CTA) or magnetic resonance angiography (MRA). In surgical planning systems and real-time visualization applications, vascular structures are commonly stored by their centerline to reduce complexity. While the surface representation, generated via marching cubes algorithm from the medical image data, is used for visualization, the centerline representation can be used to measure the distances between the vessel and other anatomical structures. Depending on the application (e.g., computational fluid dynamics), the vascular surface mesh may be highly resolved and is required to be very accurate. In contrast, high mesh resolution is critical for systems involving real-time tissue deformation, such as required for surgical simulation and training environments.

Thus, we present methods for real-time deformation of vascular trees. In section 3 we describe a physics-based deformation model utilizing centerline information. The deformation model extends a mass-spring system by additional

angular forces. For visualization, a surface can be synchronized with the centerline deformation.

Highly resolved medical surface models can be deformed in real-time, but in a complex scenario (e.g. surgical simulator), computation time is very limited. In section 4, we present a surface generation algorithm which depends on the vessel centerline and local diameter information. The resulting surface mesh has smooth transitions at the branching points of the vessel-tree. Surface deformation is performed according to the deformation of the centerline, which allows a fast and artifact-free visualization. In section 5, we present some results before we discuss the work and draw conclusions in section 6.

## 2. RELATED WORK

In medical applications, centerline representations are frequently used. A vascular tree has a complex shape because of multiple branches, changing curvature and diameter of vessels (Fig. 1). A mesh representation of the surface often requires thousands of triangles. The centerline of a vascular system is used as simplified representation for data exchange, to measure the distances and for other time consuming computations. From a geometrical perspective, the centerline is a branching lines sequence where a diameter is associated with each vertex. Additionally, the centerline with the diameter information represents the vessel's volume.

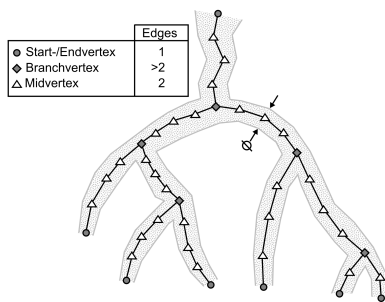


**Figure 1: 2-D projection scheme of a vascular tree. The centerline with vertices and additional diameter information represents the vessel's volume. Branch- and end-vertices support connectivity information. Thus, mid-vertices describe the vessels shape.**

One application of centerlines is the detection of similarities in shapes by comparing them [25, 14]. The centerlines represent topological connectivity as a graph, so that methods from graph theory can be applied for analysis and optimization.

Centerlines of vascular systems can be generated with various methods. For example, Montanari et al. [12] have introduced an analytical approach to compute the centerline from polygonal shapes [2, 1, 17]. Another approach in image processing is the computation of centerlines by morphological thinning of the shape [8]. Vincent et al. [23] has introduced an approach using a matrix to analyze neighboring pixels in image space. In [16] hierarchic Voronoi skeletons are introduced, which are also applicable to 3D geometries. However, the resultant skeleton is very detailed and requires additional post-processing for reduction and removal of artifacts.

As the name implies, centerlines are line structures, such as an additional surface representation is required for visualization of a vascular tree. The centerline can be achieved from an existing 3D geometry [16], but rather from binary images of anatomical data. A simple approach is to use cylinders for each line segment of the centerline. Such approximations are efficient for visualization, but they lead to surface intersections at the branches. More advanced approaches, similar to MPU Implicits [20, 21, 24] or model-based approaches like convolution surfaces [15], will prevent intersections but result in high resolution surface approximations and often requires fine tuning of several parameters for acceptable results.

For an efficient real time visualization of interactive deformable vascular trees, a low resolution surface is required with soft transitions at the branching points. Intersections between the surface mesh of connected vessels may lead to artifacts during deformation. The subsequently decimation of a high resolution surface would not only preserve surface geometry closely related to the centerline, but also details in shape, which is desired for planning purposes.

For surgical simulation or for the evaluation of residual degrees of freedom and movement space of an instrument during a possibly new intervention by experts, complex scenarios are employed. Thus, computational resources are required, e.g., for physics-based deformation of the vascular tree, tissue deformation, collision detection, or force feedback. As a consequence, high resolution surface meshes often needed to be decimated in order to reduce computational effort and to save rendering performance. It is not trivial to find an adjustments for a mesh decimation, that results in a low resolution mesh without artifacts. Once found it is not very likely that such a setup can be transferred to other vascular trees. On the other hand the centerline with diameter informations describes already the desired shape. Thus, we present a method to generate a surface mesh for visualization inspired by Scharf et al. [22] based on the centerline. The mesh has a low resolution, smooth transitions at branching points and a high quality of the faces.

## 3. PHYSICS-BASED ANIMATION

The physics-based model which we will present is motivated by the anatomical layers of vessels. The vessels boundary is subdivided in the layers intima, media and externa. The externa is a border between the vessel and surrounding tissue, whereas the intima- and media-layer are relevant for the vessel's deformation. The intima-layer contains a flexible sub-layer for flexibility longitudinal in direction of the vessel. It is distinctive in arterial vessels located close the the heart, and converts the outgoing pulse wave into a continuous blood-stream. In peripheral regions, the pulse-stream is preserved by a pulsative motion of the muscles in the media-layer. Thus, the media-layer is responsible for the perpendicular deformation of the vessel.

The centerline will be used for a physics-based deformation of a vascular tree that is visualized with a synchronized surface mesh. Thus, it is required to connect the vertices of the surface with the centerline representation. For each vertex of the surface the closest centerline segment is determined (Fig. 2) using a Sphere-Tree as hierarchical bounding volume according to Preim et al. [18].

The difference of the  $i$ -th surface vertex  $\vec{p}_i$  to its projection  $\vec{p}_i^c(\alpha)$  on the centerline yields the connection vector  $\vec{v}_i$ .

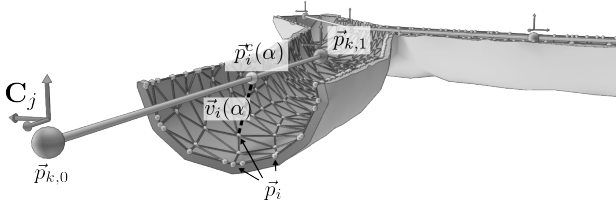


**Figure 2: Scheme of a surface and the corresponding centerline**

The projected position is represented relative to the  $k$ -th segment of the centerline, where  $\vec{p}_{k,[0,1]}$  are the vertices characterizing the segment. A change of length will also change the position of the projection point, because  $\alpha$  is defined during initialization.

$$\vec{p}_i^c(\alpha) = \vec{p}_{k,0}(1 - \alpha) + \vec{p}_{k,1}\alpha \quad (1)$$

$$\vec{v}_i = \vec{p}_i - \vec{p}_i^c(\alpha) \quad (2)$$

The intima-layer is simulated with a mass-spring system. The segments of the centerline are utilized as springs, while the mass is lumped at the centerline vertices [19]. An external force applied to one of the centerline vertices will result in internal forces until the rest length of each segment is restored. However, the mass spring system wont induce forces if the centerline is bent or the segments are rotated. This would require angular stiffness which can be induced by angular springs. Bourguignon et al. [5] have introduced a method for the computation of damped angular springs between coordinate axes to simulate anisotropic materials with tetrahedrons, which we will utilize.

Initially a local coordinate system is determined for every  $j$ -th vertex of the centerline. The orientation of the  $z$ -Axis is directed to the next segment vertex (Fig. 3, A). The  $x$ - and  $y$ -axis are not especially defined, so they can be arbitrary oriented, but the vectors must define an orthonormal base. For each local coordinate system the rotation  $\mathbf{R}_j$  to its antecessor is computed [13], such that Eq. 3 is fulfilled in the initial configuration.

$$\mathbf{C}_{j-1} = \mathbf{R}_j \mathbf{C}_j \quad (3)$$

If the vertices are move, e.g., by interaction, the segments affected by these vertices could not only be changed in length, but also rotated. This yields to a violation of Eq. 3, because the rotational matrix  $\mathbf{R}_j$  is defined during initialization and the corresponding local coordinate systems are connected by their  $z$ -axis with the segments, so that they are also rotated. The angular forces are computed with forces acting on the local coordinate systems until Eq.3 is no longer violated.

First, the coordinate system  $\mathbf{C}_j$  is transformed into the coordinate system of  $\mathbf{C}_{j-1}$  with the initially computed rotation matrix  $\mathbf{R}_j$  (Fig. 3B). Because both local coordinate systems are rotated by interaction they are not equal if  $\mathbf{C}_j$  is transformed. A regular spring is defined with a rest length of zero (Fig. 3C) between the corresponding tips of the axes of the coordinate systems. This means that the forces, applied by these regular springs will affect each pair of axes individually. In Fig. 3 forces are just applied to the  $y$ - and  $z$ -axes. The coordinate system is not rotated but the axes

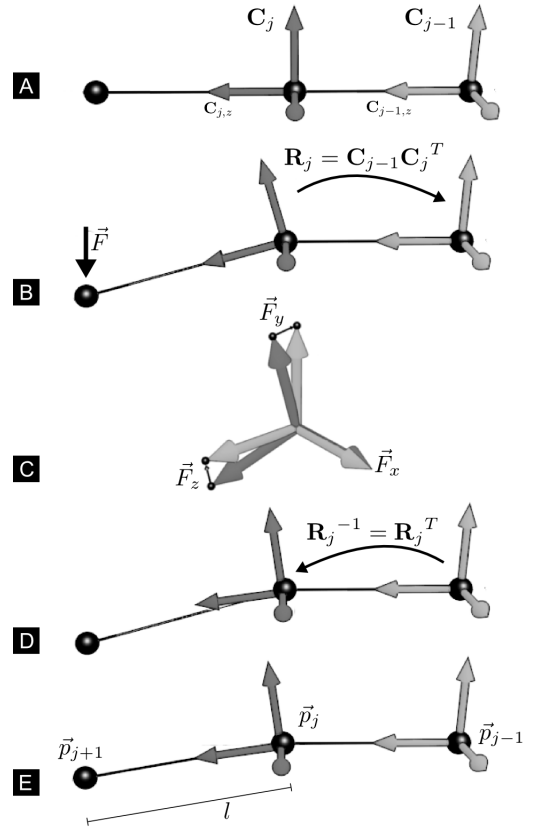


**Figure 3: Scheme for the computation of the angular forces in five steps A-E**

of the coordinate systems are reoriented by inner forces of the springs.

Until each simulation step, the axes must neither be normalized, nor perpendicular to each other so that the orthonormal base must be reconstructed. Thus, all axes are normalized and the orthogonal system is recovered by Eq.4 - 7. Thereafter, the rotation of the local coordinate system is reverted (Fig. 3, D).

$$\vec{v}_z = \vec{p}_j - \vec{p}_{j-1} \quad (4)$$

$$\mathbf{C}_{j,z} = \frac{1}{2}(\hat{v}_z + \mathbf{C}_{j,z}) \quad (5)$$

$$\mathbf{C}_{j,y} = \mathbf{C}_{j,z} \times \mathbf{C}_{j,x} \quad (6)$$

$$\mathbf{C}_{j,x} = \mathbf{C}_{j,y} \times \mathbf{C}_{j,z} \quad (7)$$

Now the angular forces are applied by the regular springs defined between the tips of the local coordinates systems. Accordingly, the segment controlled by  $\mathbf{C}_j$  is re-aligned by Eq. 8, such as  $\vec{p}_{j+1} - \vec{p}_j$  is parallel with  $\mathbf{C}_{j,z}$  (see Fig. 3E).

$$\vec{p}_{j+1} = \vec{p}_j + l \mathbf{C}_{j,z} \quad (8)$$

After the centerlines deformation is completed, the connected surface must be synchronized to the new configuration. Therefore the vector  $\vec{v}_i$  is not stored in world coordinates, but rather in the local coordinates  $\mathbf{C}_j$  and  $\mathbf{C}_{j-1}$  of the supporting centerline segment, which will yield to the

local vectors  $\vec{v}_{i,j}$  and  $\vec{v}_{i,j+1}$  (Eq. 9). It must be emphasized, that the regular springs, used to re-align the local coordinate systems are subsequently applied. The force is applied during each step of simulation and the duration of re-alignment depends on the springs stiffness. Thus, if they are not yet completely re-aligned, the world coordinates defined by  $\vec{v}_{i,j}$  in  $\mathbf{C}_j$  and  $\vec{v}_{i,j+1}$  in  $\mathbf{C}_{j+1}$  may differ. Therefore, the average between both supporting local vector are used to determine the world coordinates of the surface vertex (see Eq. 10).

$$\vec{v}_{i,j} = (\vec{v}_i \cdot \mathbf{C}_{j,x}, \vec{v}_i \cdot \mathbf{C}_{j,y}, \vec{v}_i \cdot \mathbf{C}_{j,z}) \quad (9)$$

$$\vec{p}_i = \vec{p}_i^c(\alpha) + \frac{1}{2}(\vec{v}_{i,j} + \vec{v}_{i,j+1}) \quad (10)$$

#### 4. SURFACE GENERATION

In surgical treatment planning applications, surface approximations like truncated cones [7], are commonly used, for non-pathological vessels. During deformation and bending of a vascular tree, smooth transitions at the branches are preferred.

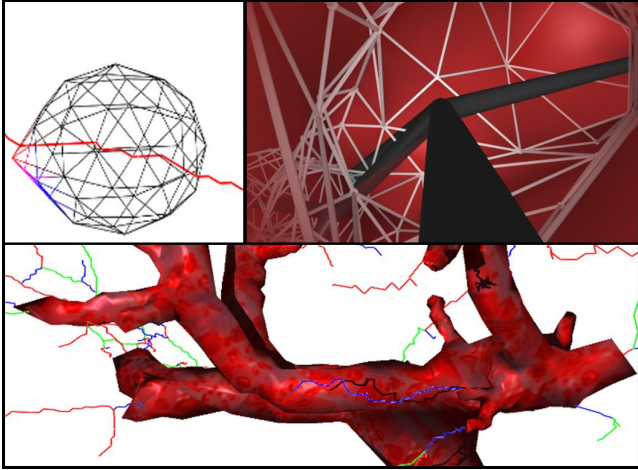


**Figure 4:** We use a geodesic sphere as seed for the growing process (top, left). The generated surface has smooth transitions at the branches and may also be used for interior visualizations (top, right). Visualization of the vascular tree surface during the generation process (bottom)

To generate a surface model with smooth transitions at branching points and appropriate mesh properties (e.g., number of triangles and triangle shape) based on given centerline and radius information, we use a geodesic sphere geometry as initial seed (Fig. 4, top left). It is placed on the branching vertex with the largest diameter, so that a large initial diameter of the seed geometry could be used. Because we are starting at a branching point, the seed will enter each vessel connected in the branching point which result in multiple branches and could be computed in parallel.

By the iteratively growth of the seed an approximation of the vessel's volume boundary is achieved. Therefore, each vertex  $\vec{v}_i$  will be moved by a force  $\vec{F}_i$ , which is defined by Eq. 11 (see also Fig. 5). The force is defined by the surface normal  $\vec{n}_i$  and an attraction force  $\vec{a}_i$  which directs from the vertex position to the closest position at the volume boundary of the vessel.

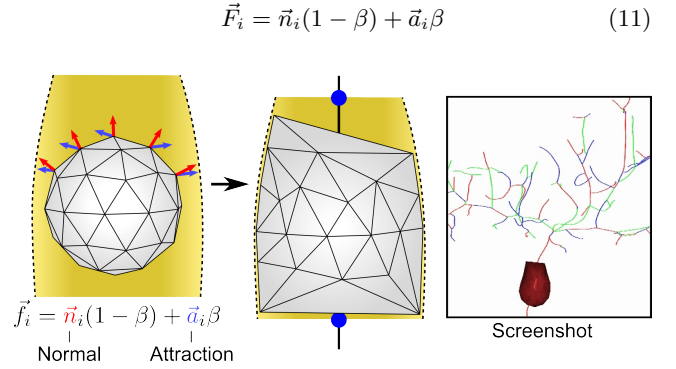


**Figure 5:** The vertices of the geodesic sphere are moved by a force composed of the vertex normal and an attraction force towards the vessels surface (left). The computation is continued, until each vertex has reached the surface defined by local diameter information (middle).

The normal will lead to an expansion of the seed, whereas the attraction force will direct the vertex movement to the volumes surface. The ratio between expansion speed and surface attraction is controlled by the weight  $\beta \in [0, 1]$ . For low values of beta the expansion is very fast and low detail is achieved longitudinal to the vessels expansion. For higher values the expansion is low, but will result in a high resolution surface. Nevertheless each vertex position is updated until it has reached the vessels surface. From an implementation point of just a small amount if vertices must be taken into account during computations.

We are using a mesh structure similar to the Winged-Edge representation [3]. Thus, each vertex contains topology information. If a vertex has reached the surface, all adjacent faces are verified. If all vertices of the face have reached the surface, the face is not in motion anymore.

If all vertices have reached the surface, the expansion can not proceed, but at branches with small vessels it could be that such vessels are not considered. Thus, if a vertex has reached the surface it adjacent faces are considered for subdivision. If one of the faces vertices are still in motion, the face is not subdivided. If all its vertices had reached the surface, it is determined if the centerline intersects with the face. If an intersection occurred the face is subdivided edge-centric. This yields to ten new faces and three additional vertices, considered as movable by Eq.11. If all vertices have reached the vessels surface and faces are not intersected by the centerline the approximation is completed.

In an additional post-processing step the generated surface is optimized. Edges are turned, if the shape is preserved and the triangle quality is increased, measured by geometrical edge- and radius-metric. Additionally, the resolution of the mesh can be increased to increase the accuracy. Therefore, the distance of the face's center to the vessels surface is computed and faces are subdivided if the distance is greater than a given threshold.

A high value for  $\beta$  in Eq. 11 will lead to a small step size longitudinal to the centerline and wont have influence on the detail of approximation detail in a cross section. Thus, small we are suggest smaller values, e.g.  $\beta = 0.3$  and an additional subdivision step.

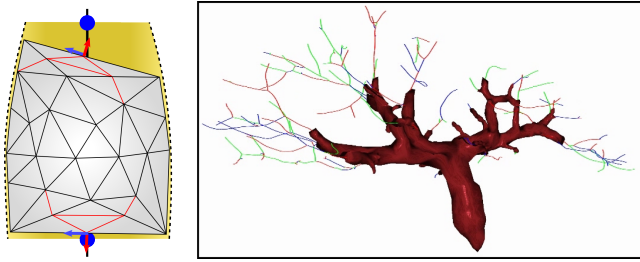


Figure 6: Faces whose vertices have reached the surface are verified. If the deviation is too large, the face is subdivided edge-centric

## 5. RESULTS

For evaluation of the performance, centerlines and meshes of different complexity were chosen. The centerlines of the vessels were extracted from CT data, segmented by medical experts. The surface in Fig. 7C was also generated by Marching Cubes from these binary images, while the surface in Fig. 7B was generated with the presented approach. Since both surfaces are related to the same centerline, a third vascular system of the liver with a more complex topology has been taken into account (Fig. 7D).

The results are summarized in Tab. 1 and illustrate that the presented approach a plausible physics based simulation of vascular trees could be achieved in real time. The visual result in Fig. 7A shows that a local force applied to a simulated vessel results in a deformation and that sharp kinks could be avoided, like it would appear if changes in rotation would not result in internal forces those are an outcome of the presented angular damped springs. Forces that result in large segment rotation were applied without the appearance of kinks or twists.

The computation performance of the physics-based simulation is adequate for interactive real-time applications, even in case of the more complex surface of the vascular tree in Fig. 7D. In case of the complex centerline in Fig. 7D, the update of the physics simulation is convincing, but the synchronization of the surface requires too much time. Indeed, the required time for synchronization is a multiple of the time required for the physics-based update. The test were made on a Intel Xeon CPU with 2,66GHz but without using possibilities for parallelization via the graphics card (CUDA) or CPU-based multi-threading.

The presented surface generation approach is easy to implement and yields surfaces with a lower mesh resolution, as marching cubes or MPU-Implicits provide. Furthermore, it results in smooth transitions at the centerlines branching points. The resulting low-resolution surface is not intended for surgical planning or computational fluid dynamics (CFD), but in surgical simulation applications, the smooth branching transitions are desired, while the performance of the simulation is essential.

Nevertheless, the surface of the vessel's volume must be approximated, so that evaluations about the required degrees of freedom during intervention can still be considered as meaningful. Thus, we compared the presented approach with respect to the resulting mesh complexity, mesh quality and accuracy of approximation.

For evaluation, we were using a data set from the livers portal vein (see Fig.7D). The centerline is more complex

and the variations in the vessel's diameter are more significant. We generated a high resolution surface using marching cubes and the centerline with diameter information from segmented anatomical data. This high resolution surface is used as reference for accuracy measurements in Tab. 2. Because the marching cubes surface is the reference for evaluation, a surface based on truncated cones is used to compare the quality of approximation.

Table 2: Comparison of our surface generation approach with marching cubes [11, 9] and truncated cones. The marching cubes surface and the centerline are generated from binary data. This centerline was utilized for the generation of surfaces with truncated cones and our approach. The Equiangle Skewness is an indicator for mesh-quality with [0,1] meaning [fine, poor].

	Number of		Equiangle Skewness		Hausdorff Distance (mm)
	Vertices	Faces	mean	max	
Marching Cubes	89.406	178.712	0,48	0.90	-
Truncated Cones	58.070	119.430	0,50	0,99	7,24
Low-Resolution	11.571	23.138	0,23	0,70	7,67
High-Resolution	51.979	103.952	0,17	0,98	7,08

Geometry: Livers portal vein

The quality of the triangles is measured by the equiangle skewness, which is the ratio between the largest and smallest inner angle in a triangle. Thus, the mean quality of the low resolution result is better than truncated cones and marching cubes. At the same time

At the same time, 20% of the vertices are used compared to truncated cones and 13% compared with marching cubes. The Hausdorff distance measures the longest distance between an approximation to the reference surface mesh based on marching cubes. Hence, a similar accuracy could be accomplished with our approach compared with truncated cones.

## 6. DISCUSSION AND CONCLUSIONS

Surface meshes generated using the presented methods are supposed to be used for visualization of vascular trees within surgical simulation systems, whereas the accuracy is sufficient compared to established methods. If a surface mesh based on truncated cones is deformed, the intersections between cones may lead to further artifacts. This, however, is avoided our method exhibiting smooth transitions at the branching points Fig. 8.

The results confirm that the presented method is suitable for interactive real-time environments and will be used in the specified scenario. The groundwork is established for the interaction with complex vascular structures and will be integrated into an environment for the virtual evaluation of minimal-invasive surgical procedures with a focusing SPT. Currently, the parametrization (stiffness, damping, mass) of the physics-based model has been done heuristically, so that the simulation is stable for update rates of at most 20ms.

For future work a parametrization based on specifically measured values is aimed. For more detailed parametrized

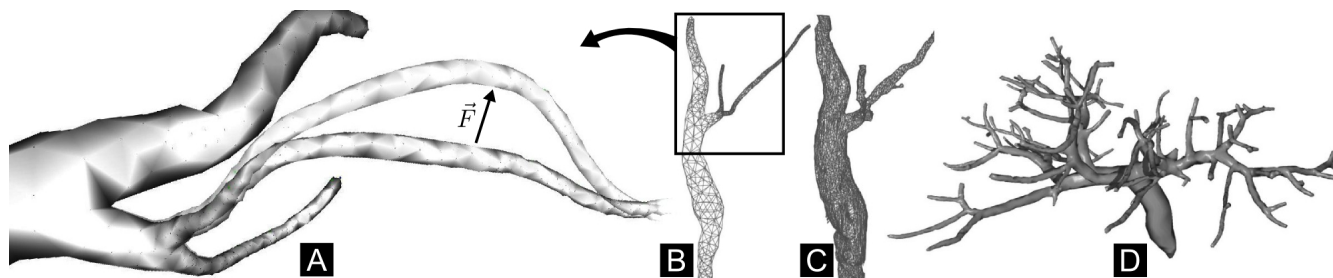


Figure 7: Results of the physics-based simulation. A Force is applied at one vessel of a vascular tree. The force was applied to a centerline connected with surfaces in (B) and (C) with different resolutions. In (A) a crossfade of initial and deformed configuration of the affected region was magnified. In (D) the data-set of a vascular tree with a more complex topology is shown.

Table 1: Summarized test results for the vascular systems in Fig. 7. The computation times for the physic based model and the time for the synchronization of the surface are feasible for interactive real-time szenarios.

	Fig. 7, B	Fig. 7, C	Fig. 7, D
Centerline (Segments, Vertices)	118/119	118/119	1559/1560
Surface (Triangles, Vertices)	2426/1215	9799/4907	25730/12867
Comp. Time			
Deformation	0,4ms (2500Hz)	0,4ms (2500Hz)	5,5ms (182Hz)
Surface Sync.	1,5ms (667Hz)	6,1ms (164Hz)	21ms (48Hz)
Total	1,9ms (536Hz)	6,5ms (154Hz)	26,5ms (38Hz)
Surface Sync. (%)	78,95%	93,85%	79,2%

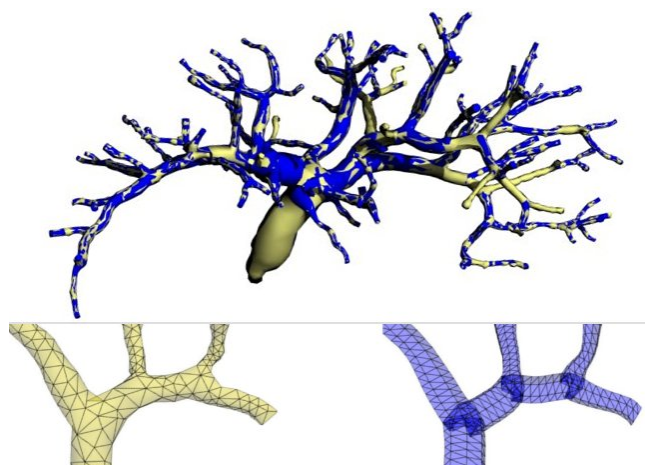


Figure 8: Overlay of surface meshes based on truncated cones (blue, bottom right) and our method (yellow, bottom left). For a static configuration, the intersections of the cones (bottom right) are covered. During movement of vessels, intersections may lead to visualization artifacts.

models, e.g., changing parameters depending on deformation for a simulation of non-linear deformations, the real time performance must be preserved. In mass spring systems, a general problem could be observed. The parameters of mass-spring systems could be achieved from young-modulus, a material parameter that could be measured from sample[4, 10]. The parametrization by measurement will define the stiffness and damping coefficient and of course the mass. Once these values are defined the stability of mass-spring

systems depends only on the update interval and the number of nodes, where the mass is lumped.

Thus, a centerline-based simulation has advantages with regard to the stability, because the centerline has less vertices compared to a synchronized surface (Fig. 7B 9,7%, Fig. 7C 2,4%). At the moment, the physics-based method allows the deformation in terms of bending. The method will be extended in future work, such that the vessel's profile can be deformed. This means that a force will not only affect the rotation of the local coordinates but also the length of the connecting vectors. An evaluation of the geometrical models and the physics-based simulation with surgeons are also preparation.

## 7. ACKNOWLEDGMENTS

The work in this paper is partially funded by the German Ministry of Education and Research (BMBF<sup>1</sup>) within the **VIERforES-II**<sup>2</sup> project (Grand no. FKZ 01IM10002A).

## 8. REFERENCES

- [1] L. Antiga, B. Ene-Iordache, and A. Remuzzi. Computational geometry for patient-specific reconstruction and meshing of blood vessels from mr and ct angiography. *IEEE Trans Med Imaging*, 22(5):674–84, 2003.
- [2] L. Antiga, M. Piccinelli, L. Botti, B. Ene-Iordache, A. Remuzzi, and D. Steinman. An image-based modeling framework for patient-specific computational hemodynamics. *Medical and Biological Engineering and Computing*, 46:1097–1112, 2008. 10.1007/s11517-008-0420-1.
- [3] B. G. Baumgart. Winged edge polyhedron representation. Technical report, Stanford University, Stanford, CA, USA, 1972.
- [4] Y. Bhasin and A. Liu. Bounds for damping that guarantee stability in mass-spring systems. *Studies in Health Technology and Informatics*, 119:55–60, 2006.
- [5] D. Bourguignon and M.-P. Cani. Controlling anisotropy in mass-spring systems. In *In Eurographics, Eurographics Assoc.*, pages 113–123. Springer-Verlag, 2000.
- [6] H. Frick, H. Leonard, and D. Starck. *Allgemeine Anatomie, Spezielle Anatomie II: Eingeweide - Nervensystem - Systematik der Muskeln und Leitungsbahnen*, volume 2 of *Taschenlehrbuch der gesamten Anatomie*. Thieme Verlag, 3. überarbeitete aufgabe edition, 1987. ISBN 3-13-356903-1.
- [7] H. Hahn, B. Preim, D. Selle, and H.-O. Peitgen. Visualization and Interaction Techniques for the Exploration of Vascular Structures. In *IEEE Visualization*, pages 395–402, San Diego, Oktober 2001.
- [8] P. Kwok. A thinning algorithm by contour generation. *Commun. ACM*, 31(11):1314–1324, 1988.
- [9] T. Lewiner, H. Lopes, and A. Vieira. Efficient implementation of marching cubes cases with topological guarantees, 2003.
- [10] B. A. Lloyd, S. Kirac, G. Székely, and M. Harders. Identification of dynamic mass spring parameters for deformable body simulation. In *Eurographics 2008 - Short Papers*, pages 131–134, 2008.
- [11] W. E. Lorensen and H. E. Cline. Marching cubes: A high resolution 3d surface construction algorithm. In *Proc. of the ACM SIGGRAPH Conference on Computer Graphics*, pages 163–169, 1987.
- [12] U. Montanari. Continuous skeletons from digitized images. *J. ACM*, 16(4):534–549, 1969.
- [13] M. Müller, J. Dorsey, L. McMillan, R. Jagnow, and B. Cutler. Stable real-time deformations. In *SCA '02: Proceedings of the 2002 ACM SIGGRAPH/Eurographics symposium on Computer animation*, pages 49–54, New York, NY, USA, 2002. ACM.
- [14] M. Náf, G. Székely, R. Kikinis, M. E. Shenton, and O. Kübler. 3d voronoi skeletons and their usage for the characterization and recognition of 3d organ shape. *Comput. Vis. Image Underst.*, 66(2):147–161, 1997.
- [15] S. Oeltze and B. Preim. Visualization of Vascular Structures: Method, Validation and Evaluation. *IEEE Transactions on Medical Imaging*, 24(4):540–548, April 2005.
- [16] R. L. Ogniewicz and O. Kübler. Hierarchic voronoi skeletons. *Pattern Recognition*, 28(3):343–359, 1995.
- [17] M. Piccinelli, A. Veneziani, D. A. Steinman, A. Remuzzi, and L. Antiga. A Framework for Geometric Analysis of Vascular Structures: Application to Cerebral Aneurysms. *IEEE Transactions on Medical Imaging*, 28(8):1141–1155, Aug. 2009.
- [18] Preim, Tietjen, and Hindennach. Integration automatischer abstandsrechnungen in die interventionsplanung. *BVM2003, Informatik aktuell*, pages 343–353, 2003.
- [19] M. Schill. *Biomechanical Soft Tissue Modeling - Techniques, Implementation and Application*. PhD thesis, Fakultät für Mathematik und Informatik, Mannheim, 02 2002.
- [20] C. Schumann, M. Neugebauer, R. Bade, B. Preim, and H.-O. Peitgen. Implicit Vessel Surface Reconstruction for Visualization and Simulation. In *International Journal of Computer Assisted Radiology and Surgery (IJCARs)*, volume 2(5), pages 275–286, 2008.
- [21] C. Schumann, S. Oeltze, R. Bade, and B. Preim. Model-free surface visualization of vascular trees. In *IEEE/Eurographics Symposium on Visualization, Eurographics*, pages 283–290, 2007.
- [22] A. Sharf, T. Lewiner, A. Shamir, and L. Kobbelt. On-the-fly curve-skeleton computation for 3d shapes. In *Eurographics 2007 (Computer Graphics Forum)*, volume 26, pages 323–328, Prague, october 2007. Eurographics.
- [23] L. Vincent. Efficient computation of various types of skeletons. In M. H. Loew, editor, *Medical Imaging V*, volume 1445, pages 297–311. SPIE, 1991.
- [24] J. Wu, M. Wei, Y. Li, X. Ma, F. Jia, and Q. Hu. Scale-adaptive surface modeling of vascular structures. *Biomed Eng Online*, 9:75, 2010.
- [25] H. Zaboli, M. Rahmati, and A. Mirzaei. Shape recognition by clustering and matching of skeletons. *Journal of Computers*, 3(5):24–33, 2008.

<sup>1</sup><http://www.bmbf.de/en/>

<sup>2</sup><http://vierfores.de>